Chapter 5

Fabrication and Characterization of Macroporous PDMS based Scaffold for Tissue Engineering

5.1 Introduction

Skin is the largest metabolic organ of the human body. It not only protects against external entities but also auto-regulates the internal environment of the body (Vig et al. 2017). In addition, it has a self-healing mechanism which begins immediately after the occurrence of a wound. However, an injury to the skin can result in severe loss of its anatomical structure and functioning. Tissue-engineered skin dressings are envisaged to provide protection to the injured site from physical damage and microbial invasion as well as to help improve the self-healing process.

Some of the techniques that are commonly used for the preparation of wound dressings suffer from various limitations. For example, it is difficult to control interconnectivity as well as pore size using gas foaming method (Zhu, Handschuh-Wang, and Zhou 2017), while electrospinning provides a limited control over the pore structures (Annabi et al. 2010). The freeze-drying method is excessively time-consuming. 3-D bioprinting, besides being costlier, lacks the ability to achieve the desired levels of mechanical strength and quite often damages the biomaterials used for fabrication (Bhardwaj, Chouhan, and Mandal 2018). Similarly, micropatterning and micro-molding techniques require a high level of skills and expertise to carry out the fabrication process. In contrast, salt leaching technique is much simpler, cheaper and does not require any specialized sophisticated equipment and expert hands. In addition, the method allows easy manipulation of pore sizes and porosity. Importantly, this method is cost effective and does not involve any harmful or toxic substance in the process of scaffold fabrication (Annabi et al. 2010). In this work, salt leaching method has been employed for the preparation of wound dressing material or a possible candidate for skin substitute. Till date, no any single material has been referred as an ideal biomaterial that can be employed as skin substitutes. For example, hydrocolloids related materials, however easy to use, severally lack gaseous

exchange and mechanical strength (Boateng et al. 2008). Similarly, hydrogels, that provide instant pain relief and are easy to remove, even require a secondary dressing material (Mir et al. 2018; Bosworth and Downes 2011). Thus, fabrication of an ideal tissue-engineered skin dressing is still known as an open problem and many efforts have been made over the past few years to investigate a range of biomaterials that could be potentially useful for designing such constructs (Vig et al. 2017).

In this chapter, we demonstrate developing a macroporous polydimethylsiloxane (PDMS) based tissue engineered skin dressing material. PDMS is a synthetic polymer of repeating chain of Si-O molecules with two methyl groups attached to silicon atoms (Caplin et al. 2015; Mou and Jiang 2017). Owing to a wide variety of attributes PDMS possesses, it has been chosen for fabricating scaffolds promising for skin dressing materials. Such properties include biocompatibility (Marom et al. 2015), non-immunogenicity, non-toxicity (Yilgör and Yilgör 2014), good mechanical strength (Aucoin et al. 2002; Bucholz, Carlton, and Holmes 1987; Heise, Osborn, and Duwe 1990; Khorasani and Mirzadeh 2004; Nunes et al. 1997; Teixeira, Ferraz, and Monteiro 2008), easy preparation and storage, easy handling, non-antigenic, prolong mean life and importantly excellent gas permeability that enables it to withstand under wound hypoxia condition as well as to restrict water loss from the wound (Zhang et al. 2009; Merkel et al. 2000). In addition, it possesses some very specific attributes desirable in a wound dressing material such as high flexibility (Yilgör and Yilgör 2014), hydrophobicity (Zhu, Handschuh-Wang, and Zhou 2017), cellular compatibility and cost-effectiveness (Bélanger and Marois 2001). In this study, we have performed co-culture of melanocytes and fibroblast cells within a 3D macroporous PDMS scaffold and thereafter evaluated its suitability for promoting cell adhesion, infiltration and proliferation. For this purpose, scaffold was first modified using plasma treatment followed by coating with an ECM protein i.e., collagen. Further, we

have assessed the cellular viability and proliferation rate of the two chosen cell types (melanocyte and fibroblast) within the scaffold. Its interconnected macroporous structure facilitates media diffusion, cellular adhesion, and proliferation within 3D scaffolds. Its permeability for gases renders the polymeric scaffold suitable for transporting oxygen and therefore facilitates gaseous exchange between the environment and damaged tissue underneath the dressing; that in turn promotes cellular growth. It may also behave as a good absorbent matrix that will help in maintaining wet conditions while removing exudate from the wound site. We have modulated porosity and mechanical properties by varying the salt to PDMS ratio which helps in achieving appropriate absorbent property and flexibility. Notably, due to the low surface energy of PDMS, it may aid atraumatic or painless removal of the entire dressing from the wound site.

5.2 Materials and methods

5.2.1 Materials

The PDMS Sylgard 184 silicone elastomer kit (Dow Corning Corporation) was used in this work. Granular food grade sodium chloride (NaCl) was purchased from SD Fine Chemicals (Mumbai, India.). Cell culture components, including DMEM high glucose (AL007A), FBS (RM9955), antibiotic penicillin (10.000 U/mL) streptomycin (10 mg/mL) (A001), trypsin–EDTA (TCL048), hydrolysed collagen type 1 (TC434), PBS (TS1101), 4% paraformaldehyde (TC119), triton X-100 (MB031), trypan blue (TC193), DAPI (TC229) and MTT assay kit (TC151) were purchased from Himedia. DMSO (TC185) was procured from Sisco Research Laboratory. 96 well plate (30096, GENETIX), sterile Petri dish 35 mm (460035, TARSON) and centrifuge tube—15 and 50 mL (GENETIX) were used for culture purposes. High analytical grade 99.9% absolute ethanol was used in performing the culture-related experiments.

5.2.2 Fabrication of macroporous PDMS scaffold

For scaffold fabrication, we employed salt leaching method. The fabrication process of PDMS scaffolds began with the formation of a firmly pressed NaCl crystal bed in a plastic mold. A sylgard 184 PDMS elastomer base mixed with a curing reagent (10:1 [w/w]) was then poured on to salt bed with different salt to prepolymer ratios (2:1 and 3:1 [w/w]). Subsequently, the mold was put in a vacuum chamber for degassing. The PDMS was then cured in a hot air oven for 4 h at 60˚C followed by peeling off the solidified PDMS salt composite from the mold. Afterwards, the composite was immersed in lukewarm de-ionized water for salt leaching. Thereafter, for further removal of the remaining salt crystals, the scaffold was subjected to ultra-sonication for 1 h. Finally, the obtained ultra-sonicated scaffold was dried in vacuum for further use (Figure 5.1).

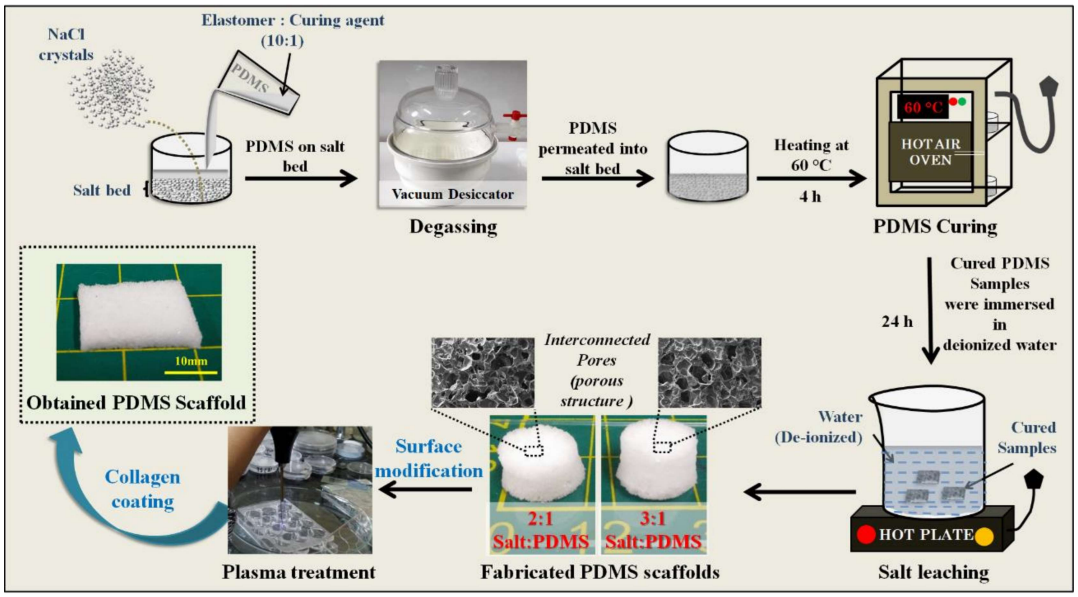

Figure 5.1 Schematic representation of porous PDMS scaffold fabrication process using salt leaching method.

5.2.3 Characterization of macroporous PDMS Scaffolds

5.2.3.1 Morphological characterization of the porous networks

The pore size distribution and morphological characteristics of the scaffolds were determined using a SEM (Zeiss EVO 18 SEM Zeiss, Oberkochen, (Germany)) with an accelerating voltage of 20 kV. Unleached and leached PDMS scaffolds were first dried in a vacuum and then cut into small thin samples. This was followed by sputter coating with gold. The obtained scaffolds were then observed under SEM to determine the extent of porosity and surface morphology. Thereafter, pore size distribution was analyzed using ImageJ software. Finally, complete removal of NaCl crystals was confirmed by examining the scaffold through energy-dispersive X-ray (EDX) spectra.

5.2.3.2 Interconnectivity of the macroporous scaffold

Fabricated scaffolds were sliced into cylindrical (10 mm diameter x 3.7 mm height) shaped samples and plasma treated followed by water soaking for 10 min. Thereafter, food color dye-water mixture was put on the upper surface of the fluid-filled samples. Next, the sample was cut into two pieces by making an incision in the middle of the scaffold to observe the dye penetration. The images were captured using a digital camera (1920 x 1080, 16.1 megapixels).

A simple setup was designed to trace and observe the transport of hydrophilic molecule within the fluid-filled PDMS scaffold. Two reservoirs R1 and R2 of equal height were set 40 mm apart with the sample placed in between the two reservoirs horizontally at the height of 5 mm from the bottom (level was ensured by a spirit level instrument) connecting both the reservoirs. The scaffold was plasma treated and soaked in water for 24 h before placing it between the reservoirs. R1 was filled with a food color dye solution while leaving R2 empty. Transport process of the dye from R1 to R2 was captured in real

time through a digital camera with a video mode (30 fps). The characteristic diffusion profile of the dye was estimated via its intensity profile across the scaffolds using Image J software.

5.2.3.3 Porosity of scaffold

The pore volume of fabricated PDMS scaffolds was quantified using a modified liquid replacement process. Cylindrical shaped (10 mm diameter × 3.7 mm height) samples were prepared from fabricated PDMS scaffold and weighed (W_{dry}). The dried porous PDMS scaffolds with ratio 2:1 and 3:1 (S: P) were submerged in EtOH (absolute). To permeate ethanol, the scaffolds were subjected to frequent cycles of vacuum and air escape in a vacuum desiccator. The ethanol saturated samples were then weighed (W_{wet}). The effective porosity (P_E) of the samples was determined as

$$P_E = \left(\frac{V_E}{V_A}\right) \times 100, \tag{5.1}$$

and V_E was calculated from the following equation:

$$V_E = \left(\frac{W_{Wet} - W_{Dry}}{\rho_{ethanol}}\right), \tag{5.2}$$

where V_E is ethanol volume, $\rho_{ethanol}$ = 0.789 g cm^{-3} is the ethanol density and V_A is the apparent volume calculated by measuring the dimensions of the scaffolds. The apparent porosity P_A was calculated theoretically as

$$P_A = \left(\frac{W_{before} - W_{after}}{W_{before}}\right) \times 100. \tag{5.3}$$

Where W_{before} and W_{after} are the weights of the samples before and after leaching, respectively.

5.2.3.4 Surface modification and wettability of scaffolds

In this study, air plasma treatment method was chosen for the surface modification of samples. Due to plasma treatment, the polymer surface gets activated by generating several functional groups on the sample surface (e.g.; hydroxyl (Lee et al. 1991; Waddell et al. 2008), carbonyl (Merenda et al. 2016), ether (Feng et al. 2006) groups etc.) resulting in an increase in the surface energy. A better understanding of surface properties can be obtained by investigating its water CAs. To measure the hydrophilicity or hydrophobicity of the solid PDMS and porous PDMS scaffolds (2:1 and 3:1), water CA was analyzed by image analysis software (ImageJ). The images were captured before and after plasma treatment using a digital camera. For every measurement, 10 μL of deionized water was dropped upon the top surface of the scaffold and an image was captured after the droplet was found stable on the surface of the scaffold. The mean value of CAs and respective SD for each type of sample were calculated by three independent tests on both sides of the sample.

5.2.3.5 Liquid holding capacity of the scaffold

In order to estimate the water holding capacity of the scaffold, we calculated the water absorption percentage of the fabricated scaffolds. The PDMS scaffolds were first dried under vacuum and then weighed to obtain W_{dry}. Thereafter, the scaffolds were plasma treated and immediately immersed in a PBS solution at a room temperature. Subsequently, after ensuring complete removal of excess water around scaffold surface through tissue paper tapping, the samples were weighed using a precision electronic balance at regular intervals of time, until the weight of samples was stabilized. The absorption percentage was determined as

$$Liquid\ Absorption\ (\%) = \left(\frac{W_{wet} - W_{dry}}{W_{dry}}\right) \times 100. \quad \textbf{(5.4)}$$

For comparison, a similar procedure was adopted to obtain the liquid absorption for non-plasma treated scaffolds to observe the efficacy of the above plasma treatment process.

5.2.3.6 Mechanical strength of scaffolds

Since compressive modulus is an essential characteristic of tissue-engineered scaffolds, the mechanical characterization of PDMS scaffolds has been addressed by compressive testing using Instron testing machine, capable of applying tensile, compressive and fatigue cycles. Cylindrical scaffolds (25 mm diameter and 15 mm thickness) were prepared and assessed for compressive testing with a cross-head speed of 5 mm/minute. Scaffold stiffness was calculated at 50% compression. The compressive modulus was quantified from the linear region of the obtained stress vs. strain graph.

5.2.3.7 Cytocompatibility Study

5.2.3.7.1 Monotypic cell culture

The L929-RFP (red fluorescent protein) mouse fibroblasts and B16-F10 murine melanocytes cells were used to mimic the physiological scenarios of the skin tissue. The fluorescence property of genetically engineered L929 cells (fluoresce red when excited at a green wavelength) was explored for identification and monitoring for cell proliferation within the scaffold under a fluorescence microscope (Nikon Ti-U). The prepared scaffolds (10 mm diameter) were first sliced into thin (<1mm) circular discs and then sterilized by autoclaving. The surface of all PDMS scaffolds was then modified through plasma treatment (BD-20 AC Laboratory Corona Treater, Electro-Technic Products, USA) for 5 min followed by collagen (hydrolyzed type 1) coating. The excess collagen was removed after 12 h and the scaffold was left to dry for 30 minutes. Both the cell lines were subcultured after attaining 80% confluency. Cells at the density of 10^5

cells were seeded separately on top of the scaffold in a 35 mm Petri dish. The cell-seeded scaffolds were kept for cell attachment in a 5% CO_2 incubator (Galaxy® 170 S, Eppendorf, Germany) at 37 ˚C for 30 minutes. Afterward, 2 mL of a complete culture medium that comprises of DMEM supplemented with 10% FBS and 1% PS was added to the Petri dish. The culture medium was replaced every alternate day. Images were captured after transferring the scaffold into new 35 mm Petri dish at various depths (bottom to top) to avoid the false imaging of cells migrated to the bottom of the flask.

5.2.3.7.2 Co-culture of fibroblasts and melanocytes within PDMS scaffolds

The co-culture system in 3D scaffolds better mimics the structure of the natural tissue in comparison to monotypic 2D culture. For co-culture, a similar procedure was adopted as in the case of in vitro monotypic cell culture. L929-RFP fibroblast cells were seeded at the density of 10^5 cells on one side of collagen coated scaffold and then left for half an hour for cell adhesion followed by the addition of 2 mL complete growth medium (DMEM + 10% FBS + 1% PS). Cell culture was maintained at 37 ˚C in a 5% CO_2 humidified incubator. After 10 days, B16-F10 melanocyte cells were seeded on the opposite side of L929-RFP fibroblast seeded scaffolds at the density of 10^5 cells per scaffold. Culture medium was changed every alternate day. The images were captured from both sides of the scaffold to visualize cell penetration of L929-RFP and B16-F10 cells at various depths. The scaffolds were flipped up and down alternatively to observe the respective cells. To visualize the nuclei of B16-F10 cells inside the scaffold in a co-culture condition, DAPI stained background corrected images of co-cultured cells were merged with the fluorescent images of L929-RFP and then transformed into their respective grayscale images using ImageJ software. Further, the grayscale images were converted into binary images at an appropriate threshold value (Mahto et al. 2014). Binary images extracted from L929-RFP fluorescent images were subtracted from the

corresponding binary image of the merged images to show the nuclei of B16-F10 cells solely.

5.2.3.7.3 Nuclear staining

To visualize the cell distribution within the scaffold, the nuclei were stained with DAPI (1µg/mL), which is a fluorescent stain that binds to A-T rich region of DNA and fluoresces blue upon excitation at a wavelength of 358 nm. Culture medium was removed from the Petri dish containing the scaffold embedded with the cells. The scaffold was then washed thrice with PBS to remove leftover media and debris content. Cells within the scaffold were fixed by adding 100 µL of 4% paraformaldehyde for 15 minutes at a room temperature followed by washing with PBS to completely remove unbound paraformaldehyde. After fixation, the cells were permeabilized for dye infusion by adding 100 µL of 0.1% (v/v) Triton X-100. After incubation for 5 minutes, scaffolds were washed thrice with PBS to prevent high degradation of the cell membrane. To block the nonspecific binding of stain, 100 µL of 1% BSA solution was added post PBS washing. Unbound BSA was removed by washing with PBS thrice followed by staining of the cells embedded within the scaffolds with DAPI (1µg/ml) and incubation for 30 minutes in a dark room to prevent stain bleaching. 50 µL glycerol (80%) was added to the scaffold to prevent cells from dehydration and finally observed under a fluorescent microscope.

5.2.3.7.4 Cell proliferation within the scaffolds

Mouse L929 fibroblastic and B16-F10 murine melanoma cell lines were obtained from IGIB, New Delhi, India, and NCCS Pune, India, respectively. Both cell lines were maintained in DMEM supplemented with 10% FBS, 1% PS antibiotic at 37^0C in a 5% CO_2 humidified incubator. Cell proliferation within the PDMS scaffolds was assayed by MTT assay. This assay is based on the principle that metabolically active cells reduce

yellow color tetrazolium MTT into intracellular purple formazan through dehydrogenase enzyme activity. This purple color formazon was quantified via spectrophotometric method after solubilization with DMSO. The rate of cell proliferation is reciprocal to the rate of tetrazolium reduction. Cell viability was calculated by the following equations

$$Cell\ viability_{test}(\%) = (Ab_{test}/Ab_{control[7day]}) \times 100, \quad \textbf{(5.5)}$$

$$Cell\ viability_{control}(\%) = (Ab_{control}/Ab_{control[7day]}) \times 100. \quad \textbf{(5.6)}$$

For this experiment, scaffolds were plasma treated followed by coating with hydrolyzed collagen (type 1) overnight (37˚C). L929 and B16F10 cells were seeded on each collagen-coated PDMS scaffold at a density of 10^4 cells/mL and incubated for 1 h in a 5% CO_2 incubator for cellular adhesion. To reduce the chances of false reading/result due to the cells that were migrated and adhered on the surface of Petri plates, we transferred scaffolds into 96-well plates for prolonged culture. Cells seeded scaffolds were then maintained in a 5% CO_2 incubator for 2, 5 and 7 days. Cells cultured without any scaffold in the wells were considered as a positive control and a complete growth medium was used as a negative control for all the experiments. After incubation, the culture medium was removed from each well and scaffolds were transferred again into new fresh wells to avoid the chances of false reading due to the cells that were migrated and adhered to the bottom of the well during incubation. A total of 100 µL MTT solution comprising of a complete growth medium (DMEM + 10% FBS + 1% PS, 90µL) and MTT (5 mg/ml in PBS, 10µL) was added to each well. After 4 h of incubation, the formazan crystals formed inside the wells were solubilized using a 100 µL DMSO solution for 15 min. After pipette-mixing, the solution mixture was transferred to the fresh wells to avoid the absorbance arising due to the scaffold. The optical absorbance was measured at 570 nm on a

multimode microplate absorbance reader (Synergy H1 hybrid, Biotek, USA). MTT assay was performed in triplicates for both cell lines along with positive controls.

5.2.3.8 Statistical analysis

At least three independent experiments ($n \geq 3$) were performed in triplicates for each of the above experiments and their results are presented as the mean ± SD. Statistical significance was performed using ANOVA with Tukey's multiple comparison tests to evaluate the difference between the groups and considered significant when $p < 0.05$ *, $p < 0.01$**, $p < 0.001$***. To remove the background noise from the fluorescent images, they were processed using ImageJ software. Gaussian blur function was applied to separately convolve the fluorescent images. The images thus obtained were subtracted from their respective original images to remove the background noise.

5.3 Results

5.3.1 Morphological characterization of the porous networks of PDMS scaffolds

Salt (NaCl) crystal free interconnected macroporous scaffold has been synthesized using a salt leaching method as it is evident from SEM micrograph and EDX spectra analysis of unleached and leached samples (Figure 5.2(a) & (b)). PDMS scaffolds, synthesized using both 2:1 and 3:1 salt: pre-polymer ratios, were found to have well-interconnected pores with even distribution all over the scaffold surface (Figure 5.2(b) & (c). Comparative pore size distribution in the above samples is shown in Figure 5.2(d). Average pore size within the scaffolds was manually measured using five images of individual samples ranging the above-defined ratios, using ImageJ software (NIH, USA) and the distribution curve was plotted using Origin software (OriginLab Corporation). The average pore size was calculated as 165.57±78.17 µm and 152.17±71.59 µm for PDMS scaffolds having ratios 2:1 and 3:1, respectively.

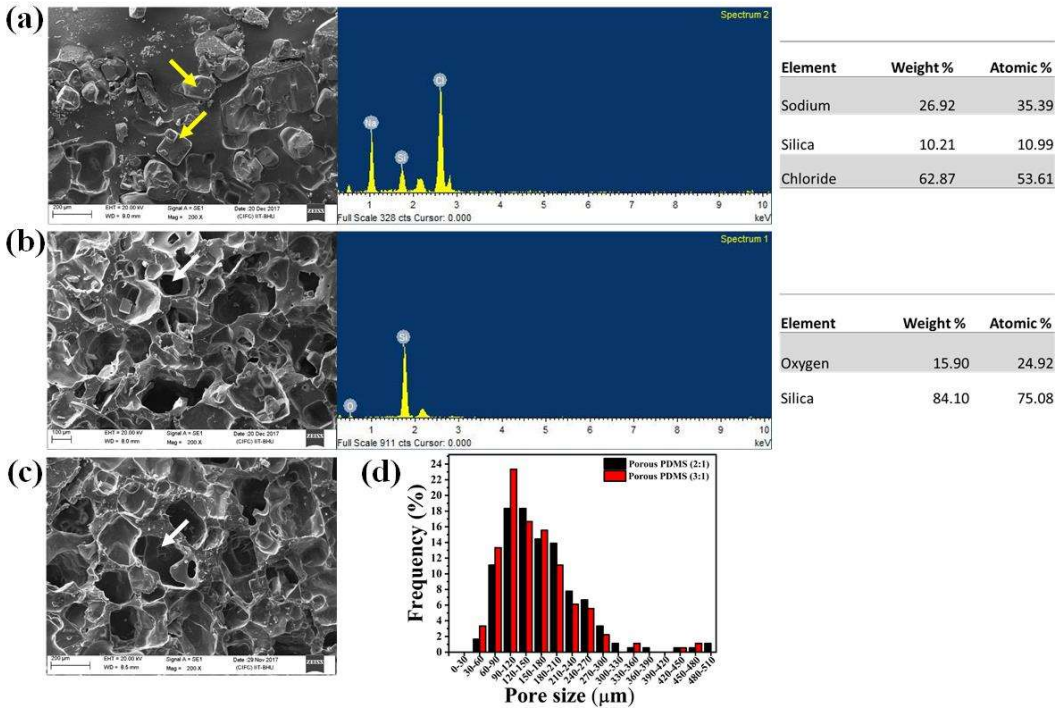

Figure 5.2 SEM micrograph of PDMS scaffolds with the corresponding EDX spectra and element analysis **(a)** before leaching and **(b)** after leaching of 2:1 PDMS scaffold, **(c)** after leaching of 3:1 PDMS scaffold and **(d)** quantitative analysis of SEM micrographs using Image J software represent wide distribution of pore size across the scaffolds. Quantitative data were calculated using at least 5 images captured from the three independent experiments.

5.3.2 Interconnectivity of the macroporous scaffold

The interconnectivity of pores within the scaffold for a skin substitute is important for oxygen, nutrient and media diffusion (Nicholas, Jeschke, and Amini-Nik 2016). Both PDMS scaffolds (2:1 and 3:1) were examined for interconnectivity of pores and found to have well-interconnected pores as both shows a significant seepage of a food coloring dye. In addition, dye permeation has been noticed significantly quicker in the case of 3:1 scaffolds in comparison to 2:1 samples (Figure 5.3(a)). It was further verified after sectioning the samples at the sagittal plane into the half. Furthermore, the characteristic diffusion profile representing for an efficient transportation of biomolecules across the entire mass of the scaffold and hence for cell growth was observed with 2:1 scaffolds.

The diffusion profile of a dye was calculated using ImageJ software and analyzed as dye intensity versus distance graph with respect to time (Figure 5.3(c)). The sample was prepared in a rectangular shape with dimensions as 40 mm × 2 mm × 1 mm. Mid portion of the sample was considered as the region of interest for calculating a diffusion profile to avoid any error in interpretation (Figure 5.3(b)). Minimum dye intensity was recorded at t=0 seconds while the maximum at t=8 seconds (Figure 5.3(c)). Representative images revealed that the dye diffused along the length of the 2:1 porous scaffold at a rate of 2 mm per second. Further, since the pore density in 3:1 sample was observed to be notably greater than that of 2:1 scaffold; the transport rate of a dye in the former was foreseen to be greater than 2 mm per second.

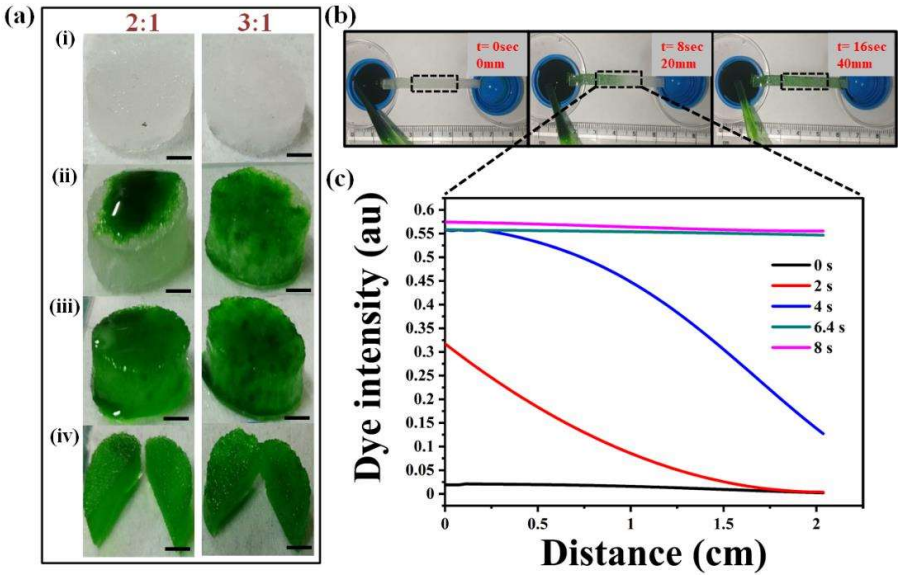

Figure 5.3 Representative micrographs reveal interconnectivity of the pores within the PDMS scaffolds **(a)** (i) plasma treated (PT) scaffolds (2:1 and 3:1 PDMS scaffold, 10 mm diameter x 3.7 mm height) imbibed with water (for t = 10 min), (ii) a food coloring dye placed on top of the water-soaked PT scaffolds, (iii) dye seepage from top to the entire volumetric space of the scaffold, (iv) cross-section of the scaffold confirming transport of the dye through the interconnected pores, **(b)** transport of the dye over time across the scaffold from a dye filled reservoir to an empty reservoir which were set 40 mm apart from each other [captured in real time using a digital camera with a video mode (30 fps)], **(c)** diffusion profile of the dye that was calculated through intensity profile across the scaffolds using an Image J software. The images were captured using a digital camera (1920 x 1080, 16.1 megapixels). Scale bar: 2.5 mm.

5.3.3 Porosity of scaffold

Porosity quantifies the number of void spaces in a material which not only provides a route for cell penetration (Sunami, Yokota, and Igarashi 2014; Phipps et al. 2012) but also acts as a template for neovascularization (Joshi et al. 2013). To determine the extent of pores developed within the fabricated PDMS scaffolds, the apparent and effective porosities of the samples were calculated. Effective porosity was measured using liquid volume retained and apparent volume of the sample. Effective porosity (P_E) denotes the ratio of interconnected void space with respect to the total volume whereas apparent porosity (P_A) is the ratio of void space (interconnected as well as non-interconnected) to the total volume. PDMS scaffold samples with 3:1 ratio were found to retain larger volume (0.175 ± 0.005 mL) compared to samples with 2:1 ratio (0.137 ± 0.009 mL) (Figure 5.4(a)). However, no significant difference was noticed between effective and apparent porosity of the respective samples (Figure 5.4(b)). The value of P_E was obtained as 52.8 ± 2.04 % and 62.9 ± 5.08 % for 2:1 and 3:1 samples, respectively. P_A of 2:1 and 3:1 PDMS scaffolds were 65.9 ± 0.41 and 75.2 ± 0.89, respectively, as represented in Table 5.1.

Table 5.1 Apparent porosity, effective porosity and volume retained for solid PDMS, porous PDMS (2:1) and porous PDMS (3:1).

Sample Name	Volume retain (mL)	Porosity (%)	
		P_A	P_E
Solid PDMS	0.003 ± 0.001	0.00 ± 0.0	1 ± 0.7
Porous PDMS(2:1)	0.137 ± 0.009	65.9 ± 0.415	52.80 ± 2.04
Porous PDMS(3:1)	0.175 ± 0.005	75.19 ± 0.8	62.90 ± 5.08

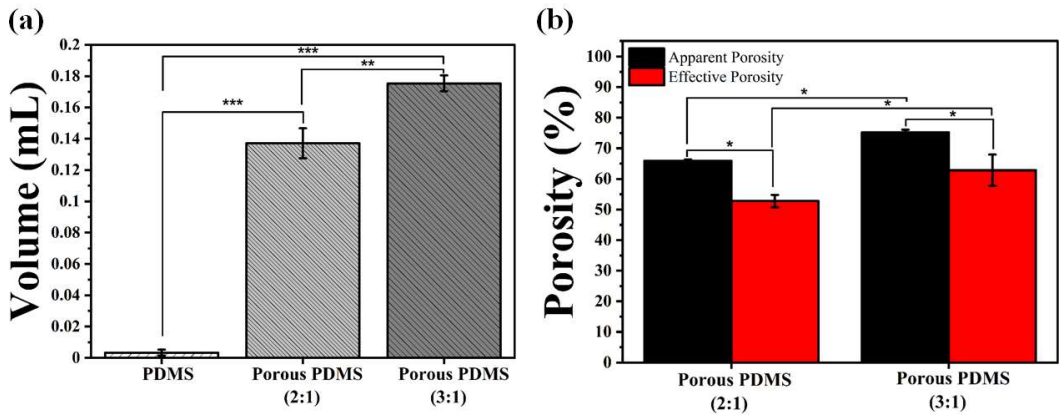

Figure 5.4 Graphs represent **(a)** the retained volume and **(b)** porosity percentage within the scaffold. Data represent mean ± standard deviation of three independent experiments. The statistical differences between the samples are represented by *$p < 0.05$; **$p < 0.01$; ***$p < 0.001$.

5.3.4 Surface modification and wettability of scaffolds

The chemical composition of surface and its microstructure geometry i.e., porosity and surface roughness can control the surface wettability property of a scaffold. To assess the effectiveness of plasma treatment, the wettability of the samples was examined by measuring the water CA. The CA value obtained for non-plasma treated porous PDMS samples (2:1 and 3:1) was significantly higher than the CA value of non-plasma treated solid samples: indicating that the surface roughness arising due to porosity might be contributing towards the hydrophobicity of the macroporous scaffolds. Moreover, both untreated (UT) solid and porous PDMS were observed to be hydrophobic most likely due to inherent hydrophobic nature of bulk PDMS (Figure 5.5). In contrast, the water drop spreads instantly and approaches to significantly lower CA on plasma-treated samples; revealing that the samples become highly wettable post-treatment of plasma.

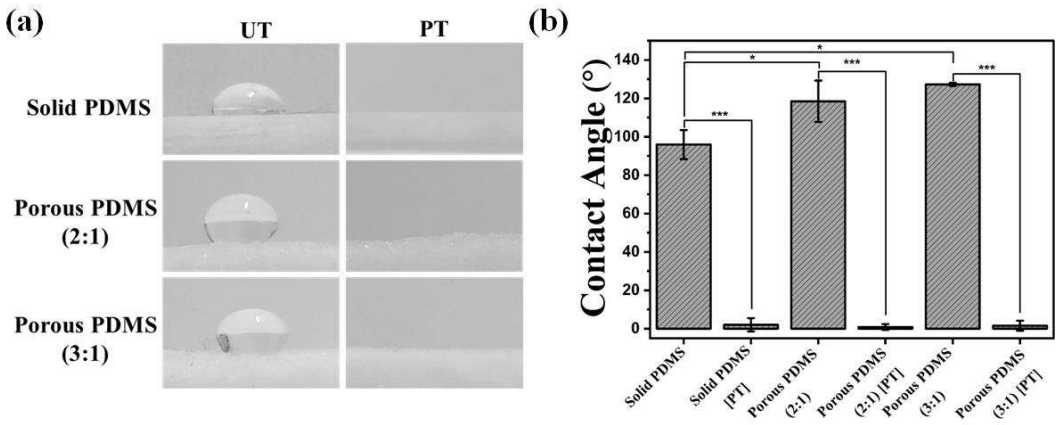

Figure 5.5 Surface water wettability of different types of the PDMS samples. **(a)** Digital images of a water droplet on different types of PDMS samples before and after plasma treatment (UT untreated, PT plasma treated) and **(b)** the CA values measured using Image J software. Data represent mean ± standard deviation of three independent experiments. The statistical differences between the samples are represented by *$p < 0.05$; **$p < 0.01$; ***$p < 0.001$.

5.3.5 Liquid holding capacity of the scaffold

Liquid absorption is one of the most important properties of the tissue-engineered scaffolds. A functional and successful scaffold must provide enough space for absorption and transport of a cell culture medium. Here, the plasma-treated (PT) samples showed a higher percentage of water absorption compared to that of non-plasma treated (UT) scaffolds during the initial 10 minutes (Figure 5.6). 2:1 and 3:1 samples (PT) showed absorption percentages of 68.5 ± 9.8% and 107.7 ± 10.3%, respectively, in the initial 10 minutes. Whereas, these values were dropped down to 12.5 ± 5.3% and 25.6 ± 2.4% for 2:1 and 3:1 samples (UT), respectively. The possible reason for this particular observation could be the hydrophobic nature of PDMS. As a result, UT samples absorbed a little amount of PBS as compared to the PT samples. After 48 h (Figure 5.6), the absorption percentage of plasma treated 2:1 and 3:1 samples was increased to 120 ± 12.6 % and 151.5 ± 7.4%, respectively. These results reveal that plasma treatment renders the PDMS

scaffold hydrophilic. Consequently, the samples get saturated with PBS solution within 10 minutes of immersion. Further, it can also be inferred from the results that the liquid absorption by the 3:1 samples is considerably higher in comparison to that of the 2:1 samples due to the availability of high void space in 3:1 samples.

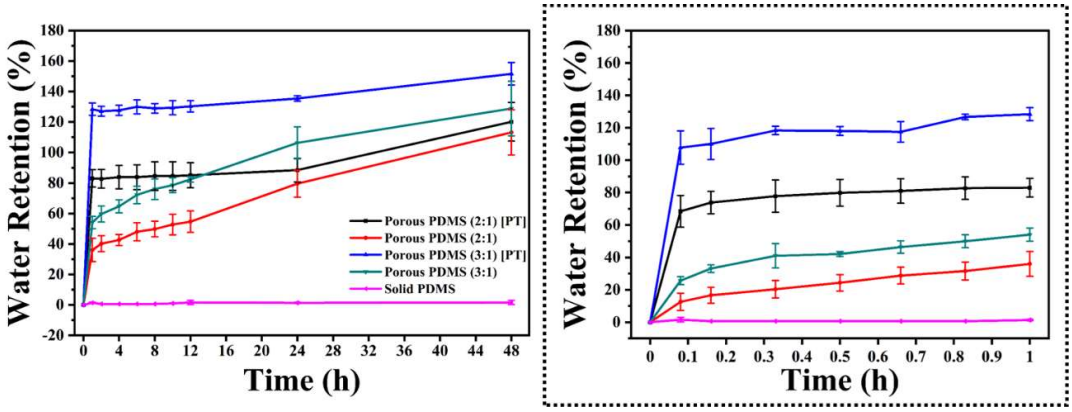

Figure 5.6 Graphs represent percentage of liquid absorption in different types of PDMS scaffolds before and after plasma treatment: after 48 h and 1 h of soaking in water. Data are presented as mean ± SD obtained through three independent experiments performed in triplicate.

5.3.6 Mechanical property of PDMS based scaffolds

The functional performance of a tissue is closely related to its mechanical strength. Mechanical properties of scaffolds control many cellular characteristics such as the viability of the cell, cell-matrix interactions, cellular phenotype, differentiation, and magnitude of the focal adhesions, hence it plays a crucial role in the development of a tissue-specific substitute (Bhardwaj, Chouhan, and Mandal 2018). The mechanical inferiority of the skin substitute often leads to fibrosis, skin contraction, and scarring in the event of a failed skin repair (Vogel 1994). Further, to check the mechanical strength, compression testing was done. Compressive modulus is an indispensable characteristic of cell scaffold. Stress-strain curves measured for different types of PDMS samples has been shown in Figure 5.7. The values of compressive modulus were calculated from the

initial linear portion of the stress-strain graph. The values obtained were 3.6 ± 0.275 MPa, 0.286 ± 0.028 MPa and 0.191 ± 0.042 MPa for solid PDMS, porous PDMS having ratios 2:1 and 3:1, respectively.

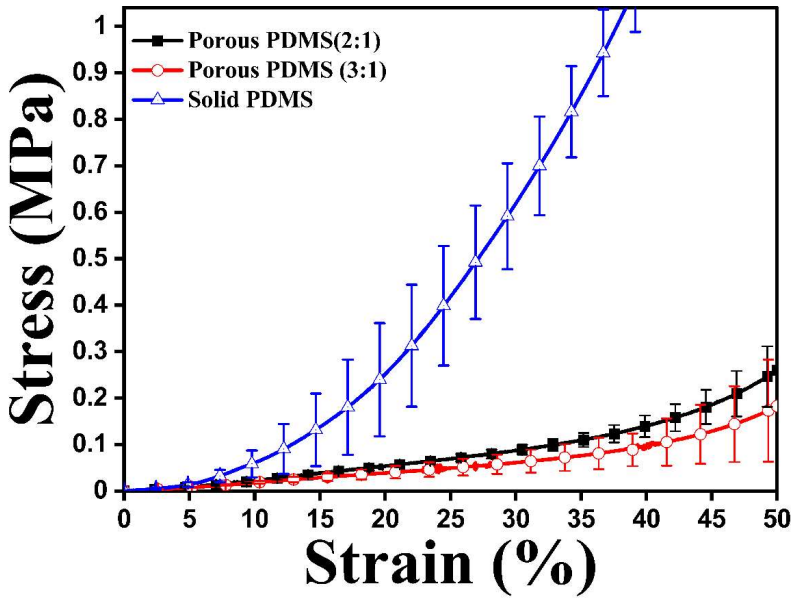

Figure 5.7 The stress–strain plot in compression for solid PDMS, porous PDMS of 2:1 and 3:1 (w/w). Data in plot represent the values of three independent experiments (n = 3).

5.3.7 Co-culture and cellular proliferation within PDMS scaffolds

In order to obtain the skin tissue level functional attributes into the scaffold, specific cells such as melanocytes and fibroblasts have been co-cultured within the scaffold. Upon fluorescence microscopy of in vitro cultured L929-RFP, we observed to the depth of ~140 μm that cells had penetrated noticeably inside the porous scaffold and formed a three-dimensional interconnected network within the scaffold (Figure 5.8(a)). The cells were found substantially interconnected after the fifth day of culture (Figure 5.8(a)) and by the fifteenth day, approximately 40% of the entire thickness of the scaffold (~560 μm) was found covered by cellular mass as analyzed by the Z-stacking images using a fluorescence microscope (Figure 5.8(c)). Spatial distribution of L929-RFP cells after 31-days of culture depicts that the porous structure of scaffold promotes the cells to form an interconnected

3D network (Figure 5.8(c)). For the ultimate procurement of 3D cellular niche and cellular adhesion, a coating of the macroporous scaffolds with collagen is known to be one of the important aspects especially when intended to mimic the skin tissue. A significant increase in the number of B16-F10 cells cultured inside the scaffold was detected by the 5^{th} day of culture as observed by a fluorescent microscope till the depth of ~90 μm (Figure 5.8(b)). The B16-F10 cell line inherently produces melanin (Chan, Kim, and Cheah 2011) and appears in the form of black spots within the culture plates (Cunha et al. 2012; Jeong et al. 2016). Tiny black spots were noticed while imaging scaffolds as well as in control (2D culture of cells in Petri plates), most likely due to the deposition of melanin pigment produced by the melanocytes. To determine the compatibility of the above cells with each other within the fabricated macroporous 3D scaffold, fluorescent images (in Z-stacking) after 20 days of co-culture were obtained using a confocal microscope (Figure 5.8(d)), wherein structures in red color represent the presence of L929-RFP cells and blue color depicts the stained nuclei of both cell types (L929-RFP and B16-F10 cells). Overlapping blue spots and red colored structures represent the nuclei of L929-RFP cells whereas non-overlapping blue color spots show nuclei of B16-F10 cells. Upon co-culturing, we found that both the cells were present in the same plane (depth ~ 180 μm) via DAPI staining. Further, both the cells were found to have migrated, adhered and proliferated deep inside the 3D space within the scaffold. To spot out the nuclei of B16-F10 cells solely, a subtraction method was implemented (Figure 5.9). In addition, nuclei staining also confirm the uniform spreading of both types of cells at discrete depths within the scaffold. No significant compromise in the physical stability and integrity of the scaffolds was noticed in the Petri dish observed until 32 days of cell culture.

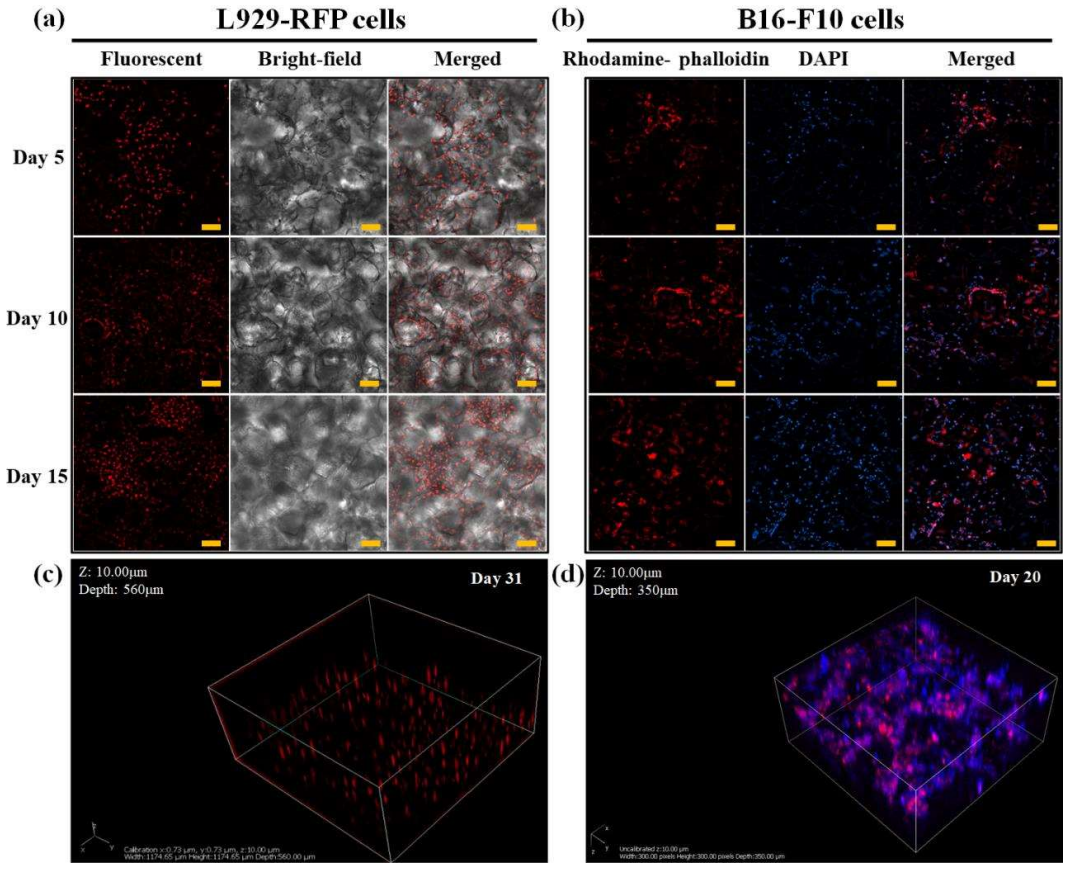

Figure 5.8 Representative images show cell culture within the PDMS based scaffolds **(a)** fluorescent intensity of L929 (fibroblast)-RFP cells observed on the various days when cultured within the PDMS scaffolds. **(b)** Rhodamine-phalloidin (F-actin) and DAPI (nuclear) stained images of B16-F10 (melanocyte) cells cultured within the PDMS scaffolds for various days. Z stacking of the image reveals the cellular network of **(c)** L929-RFP within the 560 µm thick scaffold and **(d)** co-culture of L929-RFP with B16-F10 cells using a laser confocal microscope within the 350 µm thick scaffold. Scale bar: 100 µm.

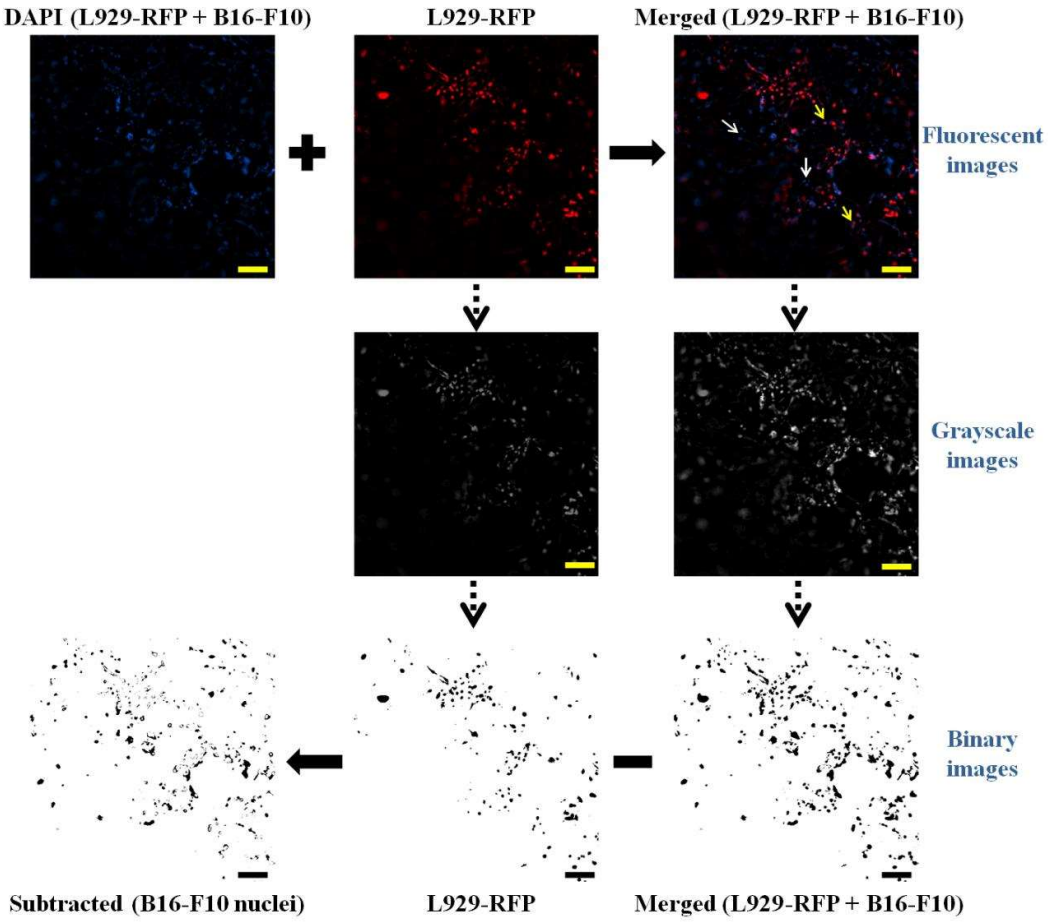

Figure 5.9 Method for showing the nuclei of B16-F10 cells in co-culture with L929-RFP using ImageJ software. Upper panel: fluorescent images of DAPI stained nuclei of both the cells (left), L929-RFP cells (middle) and merged image of first two images (right); non-overlapping blue spots exhibit the nuclei of B16-F10 cells (white arrow) and the blue spots overlapped with red mark show the nuclei of L929-RFP cells (yellow arrow). Middle panel: transformed grayscale images of L929-RFP and merged images. Lower panel: grayscale images were converted into binary images at a suitable threshold value and then subtracted to represent the nuclei of B16-F10 cells only, in a new subtracted binary image. Binary images (right to left): merged, L929-RFP and an image obtained after subtraction of L929-RFP binary image from a merged binary image that helps in the visualization of B16-F10 nuclei separately. Scale bar: 100 µm

The rate of cell proliferation (viability) within the fabricated PDMS scaffolds has been investigated using MTT assay. We calculated the percentages of cell viability within the scaffolds with respect to the absorbance of positive control observed on day 7. Data concerning the cell proliferation are presented in Figure 5.10 (a) and 5.10 (b) for L929

fibroblast and B16-F10 melanocyte, respectively. Both cell types exhibited adequate absorbance with no significant differences amongst the different kinds of porous PDMS scaffolds (2:1 and 3:1). Furthermore, cell viability was increased significantly as the culture duration increased, suggesting the suitability of both scaffolds for long-term cell culture while maintaining healthy status of the cells. The rate of cell proliferation for both cell types was observed for three different time intervals (2, 5 and 7 days). Since both cell types displayed the percentages of cell proliferation in the acceptable range, it can be ascertained that both scaffolds are supportive enough and compatible with the cells.

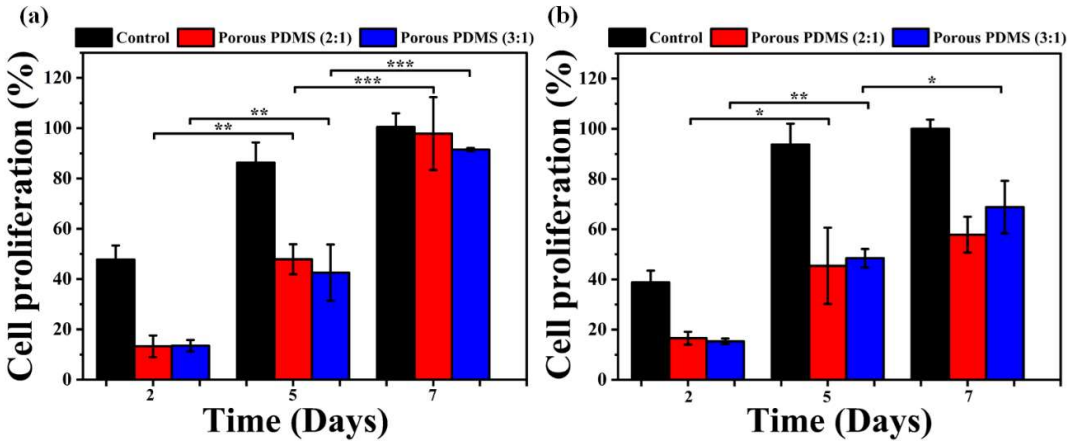

Figure 5.10 The representative graph shows cell proliferation within the PDMS based scaffold using the MTT assay (a) L929 fibroblast cells and (b) B16-F10 melanocyte cells cultured within the fabricated scaffolds with different salt to pre-polymer PDMS ratios (w/w) after 2, 5 and 7 days of culture. Cells cultured in wells (i.e., without scaffold) were considered as a control. The percentage of cell proliferation was calculated by the ratio of absorbance of test sample to the absorbance of control (at 7 days). Experiments were performed in triplicates for both cell types along with their respective controls. Data represent mean ± SD of three independent experiments. The statistical differences between the same type of scaffold at different time of culture are represented by *$p < 0.05$; **$p < 0.01$; ***$p < 0.001$.

5.4 Discussion

In this study, we developed porous PDMS sacffolds having different porosities using a salt-leaching method. The average pore size was calculated as 165.57 ± 78.17 μm and

152.17 ± 71.59 µm for PDMS scaffolds having ratios 2:1 and 3:1, respectively; indicating that varying the amount of salt resulted in no significant differences in pore size distribution of the PDMS scaffolds. However, Such noticeable and larger pores are indicative of the possibilities to facilitate increased cell migration (Sunami, Yokota, and Igarashi 2014), cell infiltration (Phipps et al. 2012), ECM secretion (Lien, Ko, and Huang 2009), and increased vascularization (Joshi et al. 2013) inside the PDMS scaffold. In addition, since the optimum range of pore sizes suitable for the growth of fibroblasts, nerve cells, and smooth muscle cells is approximately 50-160 µm (Bružauskaitė et al. 2016), it can be supported that the scaffold fabricated in this work contains pore sizes suitable for soft TE application including skin tissues. Due to the high interconnectivity of porous structures, the fabricated scaffold can serve as a wonderful absorbent and its absorbency can be modified by controlling the scaffold properties i.e., porosity and thickness. Since the ECM delivers signals that alter the unique integrin-ligand interactions between cells and their environment, the scaffold design has a direct impact on cell behavior. As a result, the environment of the 3D scaffold can either impact or control the differentiation of the cells. The mean pore size is an important factor when constructing scaffolds for any TE application. To allow cell growth, migration, and nutrient flow, scaffolds must be permeable with interconnected pores. A specific 3D space is required for cells to get the position, infiltrate, colonize in order to lay down their own ECM and niche creation to gain functional activity. If the pores are too tiny, the cells are unable to move into the construct, which limits the nutrients diffusion and waste materials elimination. This causes cells to gather around the edges of the scaffold and form a cellular capsule. On the other hand, if the pores are excessively big, there will be a reduction in the specific surface area that is accessible, which will restrict cell attachment. Additionally, the mechanical properties of the scaffold will be impaired if the pores are

too large owing to void volume (Murphy and O'Brien 2010). However, the connection between the pore size of the scaffold and the activity of the cells is not fully understood till now. Therefore, understanding of ideal pore size that is necessary for effective TE is quite limited and this is still an open topic of research. It has been demonstrated that the pore size of scaffolds affects not only the cell proliferation capacity but also the amount of ECM deposition (mainly measured by glycosaminoglycan (GAG) production and the expression of collagen gene markers), differentiation, migration, shape, and functionality of the cell (Loh and Choong 2013). However, many are reliant not just on pore size but also on other aspects including cell type, pore shape, other topographical features, overall porosity, the material of the scaffold, degradation rate of scaffold, and the environment in which the manufacturing takes place (Oh et al. 2010). Pore size is merely one of these elements.

For instance, there is considerable debate regarding the ideal pore size for osteoblast activity in tissue-engineered scaffolds. Akay et al. found that osteoblasts populated more in smaller pores (40 μm) when grown in PolyHIPE polymer (PHP) scaffolds with varying pore sizes, but larger pore sizes (100 μm) facilitated cell migration. However, varying pore sizes had little effect on mineralization (Akay, Birch, and Bokhari 2004). In (Murphy, Haugh, and O'Brien 2010), the ideal pore size of collagen-GAG (CG) scaffolds for bone TE and the impact of pore size on a preosteoblastic cell line, MC3T3-E1, were investigated. Optimal cell proliferation and infiltration were seen in CG scaffolds with mean pore sizes higher than 300 μm, and bigger pores were able to counteract the advantageous impact of larger initial cell attachment surface areas supplied by smaller pores. The effect of specific surface area was overcome in larger pores by the improved potential for cell migration and proliferation. The pore size of chondrogenic differentiation has a distinct range; pores that are either big or too tiny inhibit

development. The 100 and 200 μm pores were found to be more suitable than the 50 μm pore, which was deemed too tiny to transfer oxygen and nutrients, and the 400 μm pore, which caused excessive cell proliferation and poor differentiation capacity (Han et al. 2021). In addition, various cell types have distinct sizes and shapes, hence the ideal pore size may vary across cell types. According to a number of studies, the ideal pore size is around thirty times the size of the cell itself. During the manufacturing process of scaffolds for TE, in addition to the ideal pore size, a number of other factors, such as pore geometry, distribution pattern of pores, interconnected porosity, open or close pore, and total porosity, should be taken into consideration. All of these together have an effect on the topography, roughness, specific surface area, mechanical characteristics, and biodegradation rate of the scaffold, which in turn has an effect on the diffusion of biofluid, the initial protein adsorption, and the functions of the cells such as cell attachment, distribution, migration, and communication. Moreover, only open pore channels within the pore network facilitate cell migration, ingrowth, and the formation of vascular canals that provide blood flow to regenerative tissue.

There are various scaffold design constraints which go beyond the ideal sizes for different cell types. A number of significant factors that really must be taken into account are: when comparing in vivo research to in vitro studies, for instance, it is important to recognize that the milieu surrounding the implant is quite different from one condition to the other. In the field of biomaterials research, the process of TE makes use of a wide variety of cell types derived from a variety of species (such as mouse, rat, rabbit, and human). Hence, numerous studies have attempted to draw general inferences from single cell-biomaterial type interaction. Yet, different cells respond differently to the same biomaterial and parameter, and a single cell responds differently to multiple biomaterials and factors. Moreover, since a biodegradable implant degrades continuously, it is impossible to

maintain the regularity of the pore and overall structure. As a result, pore investigations offer only relative data since the real impacts of pores are extremely difficult to be determined.

The results indicated that scaffolds with higher salt to PDMS ratio (3:1) exhibited significantly a greater degree of porosity as compared to those with lower salt content (2:1). Therefore, the effective void volume increased notably with an increase in salt quantity during scaffold preparation. The above results were further justified by comparing the weight of samples before and after leaching from the theoretically estimated salt weight. Experimentally calculated values were found approximately similar to the estimated theoretical values. This signified that nearly all the pores formed were remarkably interconnected; hence resulted in a quite similar value of the apparent and effective porosity. The high porosity of the scaffold can facilitate loading of a variety of drugs, growth factors and other chemicals for drug delivery applications.

From the surface wettability results, it can be observed that the CA of samples increases with the rise in the levels of macroporous structures within the scaffolds (Figure 5.5 (a)). The most likely reason is an enhancement of hydrophobic property of the scaffolds due to increasing surface roughness (Lee et al. 2016). Furthermore, plasma treatment of synthesized scaffolds resulted in a significant change in water droplet shape relative to the untreated one. This suggests that surface modification through air plasma treatment significantly enhances the surface energy of each type of scaffolds (Figure 5.5). Due to the hydrophobic nature of the scaffold, it can be used as a wound dressing material that may primarily behave as a non-adherent film between the damaged tissue and dressing (Yu et al. 2013; Lee et al. 2016); rendering it remarkably suitable for atraumatic removal, particularly, to prevent suffering and further damaging tissue at the time of undressing.

The pores volume inside the scaffold plays a significant role in fluid holding; resulting in the elevated fluid holding capacity to the scaffold with higher void space (Wen et al. 2011; Chang and Hsu 2006). In the literature, it has been accepted that wet wound dressing enhances healing and also prevents scab formation in comparison to dry wound dressing (Mir et al. 2018). Further, it has also been observed that wet wound-healing results in lesser pain. Hence, considering all the outcomes together, it can be inferred that the fabricated scaffold is suitable for a wet wound dressing material.

Scaffolds having high porosity exhibited the lowest value of compressive modulus in comparison to those having low or no porosity. These results indicate that the degree of porosity and the extent of pore interconnectivity significantly influence the mechanical properties of PDMS scaffolds. Furthermore, the outcome suggests that both types of porous PDMS scaffolds exhibit the mechanical properties that are reported to be favorable for recreating the soft tissues e.g., skin (Pawlaczyk, Lelonkiewicz, and Wieczorowski 2013; C. Li et al. 2012), tendons (Maganaris and Paul 1999), smooth muscles, blood vessels (Peterson, Jensen, and Parnell 1960).

Studies over the last few years have efficiently explored the porous PDMS scaffolds for recreating tissue-engineered constructs using numerous types of cells such as human mesenchymal stem cells (Pedraza, Brady, Fraker, and Stabler 2013; Díaz Lantada et al. 2014), human adipose stem cells (J. Li et al. 2017), endothelial cells (Zargar, Nourmohammadi, and Amoabediny 2016), and pancreatic islets cells (Pedraza, Brady, Fraker, Molano, et al. 2013). However, to the best of our knowledge, there have been no reports describing the utilization of PDMS scaffolds for co-culturing of skin tissue cells towards the exploration of such scaffolds in skin TE. The incorporation of melanocytes into tissue-engineered skin substitutes provides natural color to the healed skin.

Furthermore, using melanocytes is also advantageous as it enhances the aesthetic outcomes in the healed skin (Nicholas, Jeschke, and Amini-Nik 2016). In this study, the outcomes clearly indicate the potential of PDMS scaffolds for co-culturing of cells towards skin tissue regeneration.

5.5. Summary

In this study, we have developed a macroporous PDMS scaffold that can serve as a promising material for acellular as well as cellular skin tissue dressing. In the present work, we are reporting for the first time the co-culture of B16-F10 mouse melanoma cells and L929-RFP mouse fibroblast cells in macroporous PDMS scaffolds towards the development of cellular skin tissue dressing. Scaffolds pre-coated with collagen revealed excellent biocompatibility for skin tissue-specific cells especially in terms of long-term cell culture and their proliferative potential. Cytocompatible, durable and macroporous PDMS scaffolds having different porosities with an average pore size of 160 μm were successfully fabricated using various salts to PDMS pre-polymer ratios. Fabricated scaffolds demonstrated significantly high levels of porosity and interconnectivity between the pores which can facilitate media diffusion, cellular adhesion, and proliferation within the 3D environment. Compressive modulus of the prepared scaffold was found nearly similar to that of skin tissue that renders them a good fit for skin tissue regeneration. The versatile tunability of the PDMS scaffold in terms of porosity, interconnectivity, mechanical properties renders them an appropriate candidate for various applications in the areas of tissue engineering and drug delivery, including in vivo implantation, in vitro disease model and wound dressing material. Additional information towards future applications of the fabricated scaffold may be obtained by conducting in vivo experiments. Results from such investigations will provide better insights while validating their compatibility properties in comparison to their in vitro counterparts.

Altogether, this study lays the groundwork for the future work focused on the use of the PDMS platform towards developing tissue-engineered skin wound dressing.

5.6 References

Akay, G., M. A. Birch, and M. A. Bokhari. 2004. “Microcellular PolyHIPE Polymer Supports Osteoblast Growth and Bone Formation in Vitro.” Biomaterials 25 (18): 3991–4000. https://doi.org/10.1016/j.biomaterials.2003.10.086.

Annabi, Nasim, Jason W. Nichol, Xia Zhong, Chengdong Ji, Sandeep Koshy, Ali Khademhosseini, and Fariba Dehghani. 2010. “Controlling the Porosity and Microarchitecture of Hydrogels for Tissue Engineering.” *Tissue Engineering. Part B, Reviews* 16 (4): 371–83. https://doi.org/10.1089/ten.TEB.2009.0639.

Aucoin, L., C. M. Griffith, G. Pleizier, Y. Deslandes, and H. Sheardown. 2002. “Interactions of Corneal Epithelial Cells and Surfaces Modified with Cell Adhesion Peptide Combinations.” *Journal of Biomaterials Science. Polymer Edition* 13 (4): 447–62.

Bélanger, M. C., and Y. Marois. 2001. “Hemocompatibility, Biocompatibility, Inflammatory and in Vivo Studies of Primary Reference Materials Low-Density Polyethylene and Polydimethylsiloxane: A Review.” *Journal of Biomedical Materials Research* 58 (5): 467–77.

Bhardwaj, Nandana, Dimple Chouhan, and Biman B. Mandal. 2018. “14 - 3D Functional Scaffolds for Skin Tissue Engineering.” In *Functional 3D Tissue Engineering Scaffolds*, 345–65. Woodhead Publishing. https://doi.org/10.1016/B978-0-08-100979-6.00014-8.

Boateng, Joshua S., Kerr H. Matthews, Howard N. E. Stevens, and Gillian M. Eccleston. 2008. “Wound Healing Dressings and Drug Delivery Systems: A Review.” *Journal of Pharmaceutical Sciences* 97 (8): 2892–2923. https://doi.org/10.1002/jps.21210.

Bosworth, L., and S. Downes. 2011. *Electrospinning for Tissue Regeneration*. Elsevier.

Bružauskaitė, Ieva, Daiva Bironaitė, Edvardas Bagdonas, and Eiva Bernotienė. 2016. “Scaffolds and Cells for Tissue Regeneration: Different Scaffold Pore Sizes-Different Cell Effects.” *Cytotechnology* 68 (3): 355–69. https://doi.org/10.1007/s10616-015-9895-4.

Bucholz, R. W., A. Carlton, and R. E. Holmes. 1987. “Hydroxyapatite and Tricalcium Phosphate Bone Graft Substitutes.” *The Orthopedic Clinics of North America* 18 (2): 323–34.

Caplin, Jeremy D., Norma G. Granados, Myra R. James, Reza Montazami, and Nastaran Hashemi. 2015. “Microfluidic Organ-on-a-Chip Technology for Advancement of Drug Development and Toxicology.” *Advanced Healthcare Materials* 4 (10): 1426–50. https://doi.org/10.1002/adhm.201500040.

Chan, Y. Y., K. H. Kim, and S. H. Cheah. 2011. “Inhibitory Effects of Sargassum Polycystum on Tyrosinase Activity and Melanin Formation in B16F10 Murine Melanoma Cells.” *Journal of Ethnopharmacology* 137 (3): 1183–88. https://doi.org/10.1016/j.jep.2011.07.050.

Chang, Chih Pong, and Che Chang Hsu. 2006. “The Formation and Water Content of Synthetic Fiber Growing Media.” *Materials Science and Engineering: A* 433 (1): 100–103. https://doi.org/10.1016/j.msea.2006.07.025.

Cunha, Elizabeth S., Rebeca Kawahara, Marina K. Kadowaki, Hudson G. Amstalden, Guilhermina R. Noleto, Silvia Maria S. C. Cadena, Sheila M. B. Winnischofer, and Glaucia R. Martinez. 2012. “Melanogenesis Stimulation in B16-F10 Melanoma Cells Induces Cell Cycle Alterations, Increased ROS Levels and a Differential Expression of Proteins as Revealed by Proteomic Analysis.” *Experimental Cell Research* 318 (15): 1913–25. https://doi.org/10.1016/j.yexcr.2012.05.019.

Díaz Lantada, Andrés, Hernán Alarcón Iniesta, Beatriz Pareja Sánchez, and Josefa Predestinación García-Ruíz. 2014. “Free-Form Rapid Prototyped Porous PDMS Scaffolds Incorporating Growth Factors Promote Chondrogenesis.” *Advances in Materials Science and Engineering* 2014: 1–10. https://doi.org/10.1155/2014/612976.

Han, Yu, Meifei Lian, Qiang Wu, Zhiguang Qiao, Binbin Sun, and Kerong Dai. 2021. “Effect of Pore Size on Cell Behavior Using Melt Electrowritten Scaffolds.” Frontiers in Bioengineering and Biotechnology 9. https://www.frontiersin.org/articles/10.3389/fbioe.2021.629270.

Heise, U., J. F. Osborn, and F. Duwe. 1990. “Hydroxyapatite Ceramic as a Bone Substitute.” *International Orthopaedics* 14 (3): 329–38.

Jeong, Yun Gyu, Jin Sil Lee, Jae Kwon Shim, and Won Hur. 2016. “A Scaffold-Free Surface Culture of B16F10 Murine Melanoma Cells Based on Magnetic Levitation.” *Cytotechnology* 68 (6): 2323–34. https://doi.org/10.1007/s10616-016-0026-7.

Joshi, Vaidehi S., Nan Ye Lei, Christopher M. Walthers, Benjamin Wu, and James C. Y. Dunn. 2013. “Macroporosity Enhances Vascularization of Electrospun Scaffolds.” *Journal of Surgical Research* 183 (1): 18–26. https://doi.org/10.1016/j.jss.2013.01.005.

Khorasani, M. T., and H. Mirzadeh. 2004. “Laser Surface Modification of Silicone Rubber to Reduce Platelet Adhesion in Vitro.” *Journal of Biomaterials Science. Polymer Edition* 15 (1): 59–72.

Lee, Ethan, Hongbin Zhang, John K. Jackson, Chinten James Lim, and Mu Chiao. 2016. “Janus Films with Stretchable and Waterproof Properties for Wound Care and Drug Delivery Applications.” *RSC Advances* 6 (83): 79900–909. https://doi.org/10.1039/C6RA16232K.

Li, Chunhui, Guangying Guan, Roberto Reif, Zhihong Huang, and Ruikang K. Wang. 2012. “Determining Elastic Properties of Skin by Measuring Surface Waves from an Impulse Mechanical Stimulus Using Phase-Sensitive Optical Coherence Tomography.” *Journal of The Royal Society Interface* 9 (70): 831–41. https://doi.org/10.1098/rsif.2011.0583.

Li, Jianfeng, Xiao Liu, Jeremy M. Crook, and Gordon G. Wallace. 2017. “Development of a Porous 3D Graphene-PDMS Scaffold for Improved Osseointegration.” *Colloids and Surfaces B: Biointerfaces* 159 (November): 386–93. https://doi.org/10.1016/j.colsurfb.2017.07.087.

Lien, Sio-Mei, Liang-Yu Ko, and Ta-Jen Huang. 2009. “Effect of Pore Size on ECM Secretion and Cell Growth in Gelatin Scaffold for Articular Cartilage Tissue Engineering.” *Acta Biomaterialia* 5 (2): 670–79. https://doi.org/10.1016/j.actbio.2008.09.020.

Loh, Qiu Li, and Cleo Choong. 2013. “Three-Dimensional Scaffolds for Tissue Engineering Applications: Role of Porosity and Pore Size.” Tissue Engineering. Part B, Reviews 19 (6): 485–502. https://doi.org/10.1089/ten.TEB.2012.0437.

Maganaris, Constantinos N, and John P Paul. 1999. “In Vivo Human Tendon Mechanical Properties.” *The Journal of Physiology* 521 (Pt 1): 307–13. https://doi.org/10.1111/j.1469-7793.1999.00307.x.

Marom, Anat, Sanjeev Kumar Mahto, Erez Shor, Janna Tenenbaum-Katan, Josué Sznitman, and Shy Shoham. 2015. “Microfluidic Chip for Site-Specific Neuropharmacological Treatment and Activity Probing of 3D Neuronal ‘Optonet’ Cultures.” *Advanced Healthcare Materials* 4 (10): 1478–83, 1422. https://doi.org/10.1002/adhm.201400643.

Merkel, T. C., V. I. Bondar, K. Nagai, B. D. Freeman, and I. Pinnau. 2000. “Gas Sorption, Diffusion, and Permeation in Poly(Dimethylsiloxane).” *Journal of Polymer Science Part B: Polymer Physics* 38 (3): 415–34. https://doi.org/10.1002/(SICI)1099-0488(20000201)38:3<415::AID-POLB8>3.0.CO;2-Z.

Mir, Mariam, Murtaza Najabat Ali, Afifa Barakullah, Ayesha Gulzar, Munam Arshad, Shizza Fatima, and Maliha Asad. 2018. “Synthetic Polymeric Biomaterials for Wound Healing: A Review.” *Progress in Biomaterials* 7 (1): 1–21. https://doi.org/10.1007/s40204-018-0083-4.

Mou, Lei, and Xingyu Jiang. 2017. “Materials for Microfluidic Immunoassays: A Review.” *Advanced Healthcare Materials* 6 (15). https://doi.org/10.1002/adhm.201601403.

Murphy, Ciara M., Matthew G. Haugh, and Fergal J. O’Brien. 2010. “The Effect of Mean Pore Size on Cell Attachment, Proliferation and Migration in Collagen-Glycosaminoglycan Scaffolds for Bone Tissue Engineering.” Biomaterials 31 (3): 461–66. https://doi.org/10.1016/j.biomaterials.2009.09.063.

Murphy, Ciara M, and Fergal J O’Brien. 2010. “Understanding the Effect of Mean Pore Size on Cell Activity in Collagen-Glycosaminoglycan Scaffolds.” Cell Adhesion & Migration 4 (3): 377–81. https://doi.org/10.4161/cam.4.3.11747.

Nicholas, Mathew N., Marc G. Jeschke, and Saeid Amini-Nik. 2016. “Methodologies in Creating Skin Substitutes.” *Cellular and Molecular Life Sciences: CMLS* 73 (18): 3453–72. https://doi.org/10.1007/s00018-016-2252-8.

Nunes, C. R., S. J. Simske, R. Sachdeva, and L. M. Wolford. 1997. “Long-Term Ingrowth and Apposition of Porous Hydroxylapatite Implants.” *Journal of Biomedical Materials*

Research 36 (4): 560–63. https://doi.org/10.1002/(SICI)1097-4636(19970915)36:4<560::AID-JBM15>3.0.CO;2-E.

Oh, Se Heang, Tae Ho Kim, Gun Il Im, and Jin Ho Lee. 2010. "Investigation of Pore Size Effect on Chondrogenic Differentiation of Adipose Stem Cells Using a Pore Size Gradient Scaffold." Biomacromolecules 11 (8): 1948–55. https://doi.org/10.1021/bm100199m.

Pawlaczyk, Mariola, Monika Lelonkiewicz, and Michał Wieczorowski. 2013. "Age-Dependent Biomechanical Properties of the Skin." *Advances in Dermatology and Allergology/Postępy Dermatologii i Alergologii* 30 (5): 302–6. https://doi.org/10.5114/pdia.2013.38359.

Pedraza, Eileen, Ann-Christina Brady, Christopher A. Fraker, R. Damaris Molano, Steven Sukert, Dora M. Berman, Norma S. Kenyon, Antonello Pileggi, Camillo Ricordi, and Cherie L. Stabler. 2013. "Macroporous Three-Dimensional PDMS Scaffolds for Extrahepatic Islet Transplantation." *Cell Transplantation* 22 (7): 1123–35. https://doi.org/10.3727/096368912X657440.

Pedraza, Eileen, Ann-Christina Brady, Christopher A. Fraker, and Cherie L. Stabler. 2013. "Synthesis of Macroporous Poly(Dimethylsiloxane) Scaffolds for Tissue Engineering Applications." *Journal of Biomaterials Science, Polymer Edition* 24 (9): 1041–56. https://doi.org/10.1080/09205063.2012.735097.

Peterson, L. H., R. E. Jensen, and J. Parnell. 1960. "Mechanical Properties of Arteries in Vivo." *Circulation Research* 8 (3): 622–39. https://doi.org/10.1161/01.RES.8.3.622.

Phipps, Matthew C., William C. Clem, Jessica M. Grunda, Gregory A. Clines, and Susan L. Bellis. 2012. "Increasing the Pore Sizes of Bone-Mimetic Electrospun Scaffolds Comprised of Polycaprolactone, Collagen I and Hydroxyapatite to Enhance Cell Infiltration." *Biomaterials* 33 (2): 524–34. https://doi.org/10.1016/j.biomaterials.2011.09.080.

Sunami, Hiroshi, Ikuko Yokota, and Yasuyuki Igarashi. 2014. "Influence of the Pattern Size of Micropatterned Scaffolds on Cell Morphology, Proliferation, Migration and F-Actin Expression." *Biomaterials Science* 2 (3): 399–409. https://doi.org/10.1039/C3BM60237K.

Teixeira, Sandra, Maria Pia Ferraz, and Fernando J. Monteiro. 2008. “Biocompatibility of Highly Macroporous Ceramic Scaffolds: Cell Adhesion and Morphology Studies.” *Journal of Materials Science. Materials in Medicine* 19 (2): 855–59. https://doi.org/10.1007/s10856-007-3005-x.

Vig, Komal, Atul Chaudhari, Shweta Tripathi, Saurabh Dixit, Rajnish Sahu, Shreekumar Pillai, Vida A. Dennis, and Shree R. Singh. 2017. “Advances in Skin Regeneration Using Tissue Engineering.” *International Journal of Molecular Sciences* 18 (4). https://doi.org/10.3390/ijms18040789.

Vogel, H. G. 1994. “Mechanical Measurements of Skin.” *Acta Dermato-Venereologica. Supplementum* 185: 39–43.

Wen, Pu, Jianping Gao, Yongli Zhang, Xiulan Li, Ying Long, Xinhua Wu, Yang Zhang, et al. 2011. “Fabrication of Chitosan Scaffolds with Tunable Porous Orientation Structure for Tissue Engineering.” *Journal of Biomaterials Science. Polymer Edition* 22 (1–3): 19–40. https://doi.org/10.1163/092050609X12572464984331.

Yilgör, Emel, and Iskender Yilgör. 2014. “Silicone Containing Copolymers: Synthesis, Properties and Applications.” *Progress in Polymer Science*, Topical issue on Polymer Chemistry, 39 (6): 1165–95. https://doi.org/10.1016/j.progpolymsci.2013.11.003.

Yu, Dongmei, Yunhui Zhao, Hui Li, Hengzhi Qi, Bo Li, and Xiaoyan Yuan. 2013. “Preparation and Evaluation of Hydrophobic Surfaces of Polyacrylate-Polydimethylsiloxane Copolymers for Anti-Icing.” *Progress in Organic Coatings* 76 (10): 1435–44. https://doi.org/10.1016/j.porgcoat.2013.05.036.

Zargar, Reyhaneh, Jhamak Nourmohammadi, and Ghassem Amoabediny. 2016. “Preparation, Characterization, and Silanization of 3D Microporous PDMS Structure with Properly Sized Pores for Endothelial Cell Culture: Application of 3D Microporous PDMS Structure.” *Biotechnology and Applied Biochemistry* 63 (2): 190–99. https://doi.org/10.1002/bab.1371.

Zhang, Yuhua, Masatoshi Ishida, Yutaka Kazoe, Yohei Sato, and Norihisa Miki. 2009. “Water-Vapor Permeability Control of PDMS by the Dispersion of Collagen Powder.” *IEEJ Transactions on Electrical and Electronic Engineering* 4 (3): 442–49. https://doi.org/10.1002/tee.20429.

Zhu, Deyong, Stephan Handschuh-Wang, and Xuechang Zhou. 2017. “Recent Progress in Fabrication and Application of Polydimethylsiloxane Sponges.” *Journal of Materials Chemistry A* 5 (32): 16467–97. https://doi.org/10.1039/C7TA04577H.